

Binding and dimerization control phase separation in a compartment

Riccardo Rossetto,^{1,2} Gerrit Wellecke,^{1,2} and David Zwicker^{1,*}

¹*Max Planck Institute for Dynamics and Self-Organization, Am Faßberg 17, 37077 Göttingen, Germany*

²*University of Göttingen, Institute for the Dynamics of Complex Systems,
Friedrich-Hund-Platz 1, 37077 Göttingen, Germany*

(Dated: July 23, 2024)

Biological cells exhibit a hierarchical spatial organization, where various compartments harbor condensates that form by phase separation. Cells can control the emergence of these condensates by affecting compartment size, the amount of the involved molecules, and their physical interactions. While physical interactions directly affect compartment binding and phase separation, they can also cause oligomerization, which has been suggested as a control mechanism. Analyzing an equilibrium model, we illustrate that oligomerization amplifies compartment binding and phase separation, which reinforce each other. This nonlinear interplay can also induce multistability, which provides additional potential for control. Our work forms the basis for deriving thermodynamically consistent kinetic models to understand how biological cells can regulate phase separation in their compartments.

I. INTRODUCTION

Biological cells face the difficult challenge of controlling the spatial organization of their biomolecules. They partly meet this challenge by compartmentalization, where lipid membranes or other well-defined structures physically separate the cytosol into chemically-distinct regions. Within each compartment, spontaneous accumulation of biomolecules, in particular via phase separation [1], can impart further organization. Examples for these hierarchical organizations encompass compartments of various spatial dimension; see Fig. 1a. One example for a linear, 1D compartment is the synaptonemal complex (SC), a liquid-crystalline compartment forming between homologous chromosomes during meiosis [2], which binds molecules that can then diffuse along it and accumulate in small foci [3–5]. Protein accumulation on DNA might be another example for a similar 1D structure [6]. Less speculative is the formation of protein-rich domains in 2D lipid membranes [7]. These domains are thought to form by phase separation [8–11], and the involved proteins can exchange with the bulk cytosol [12] or with separated membrane regions [13–15]. Finally, there are many examples of 3D compartments, either membrane-bound, like the nucleus, or membrane-less, like the nucleolus, which can harbor phase-separating proteins [16]. These examples show that cells employ an hierarchical organization, combining spontaneous phase separation with binding to existing compartments.

Biological cells also face the difficulty to respond to external stimuli and deploy appropriate responses. In our context, this implies that cells control phase separation in compartments. While they can regulate the amount of material to control whether phase separation takes place [1], a faster, and presumably more efficient, approach is to regulate the physical properties of the

involved molecules, e.g., by post-translational modifications [17]. On the one hand, molecular properties directly affect the affinity toward a compartment and phase separation. On the other hand, specific physical interactions between proteins might lead to the formation of small oligomers, which could affect these processes. Indeed, there is experimental evidence that oligomerization regulates protein domains on membranes [9, 18–20]. The aim of this paper is to disentangle the respective contributions of compartment binding, unspecific interactions, and oligomerization on phase separation in compartments.

Biological cells are alive, implying that many processes are driven away from equilibrium, which could also affect protein domains in compartments. Previous work has described such systems using kinetic models [21, 22], reaction-diffusion equations [23–26], and coupled Cahn-Hilliard equations [27, 28]. However, these phenomenological models do not take into account thermodynamic constraints, so they cannot reveal the precise influence of the physical properties of the involved molecules. Thermodynamically-consistent models have been derived for the specific case of wetting and pre-wetting on a membrane with surface binding [29, 30], but a more general theory is missing. In this paper, our aim is to unveil thermodynamic principles of phase separation in compartments based on an equilibrium model; see Fig. 1b. After introducing the model, we discuss in the subsequent sections the interplay between compartment binding, unspecific interactions, and dimerization as an example of oligomerization.

II. EQUILIBRIUM MODEL OF PHASE SEPARATION IN A COMPARTMENT

Our model describes solute molecules in a compartment of fixed volume V_c coupled to a larger bulk of volume V_b . To account for different morphologies (see Fig. 1a), the dimension n of the compartment can dif-

* david.zwicker@ds.mpg.de

fer from the dimension m of the bulk, implying that V_c and V_b may have different units. Each subsystem is filled with a liquid mixture consisting of a solvent and a solute, which can form dimers. The state of the compartment is characterized by the volume fraction fields $\phi_1(\mathbf{r})$ and $\phi_2(\mathbf{r})$ for the solute monomers and dimers, respectively, whereas the solvent fraction is $1 - \phi_1 - \phi_2$. Analogously, the state of the bulk is described by fields $\psi_1(\mathbf{r})$ and $\psi_2(\mathbf{r})$. Material conservation implies the constraint

$$\frac{1}{\nu_c} \int_{V_c} (\phi_1 + \phi_2) d^n r + \frac{1}{\nu_b} \int_{V_b} (\psi_1 + \psi_2) d^m r = N_{\text{tot}}, \quad (1)$$

where N_{tot} is the total number of solute molecules with molecular volumes ν_c and ν_b in the compartment and bulk, respectively. Introducing the total fraction of solute in the compartment, $\phi = \phi_1 + \phi_2$, and the total fraction in the bulk, $\psi = \psi_1 + \psi_2$, material conservation becomes

$$\eta \bar{\psi} + \bar{\phi} = \Phi_{\text{tot}}, \quad (2)$$

where $\bar{\phi} = V_c^{-1} \int \phi d^n r$ and $\bar{\psi} = V_b^{-1} \int \psi d^m r$ are the average total fractions in the respective subsystems. The relative size of the subsystems is $\eta = (\nu_c V_b) / (\nu_b V_c)$, where $\eta > 1$ when the bulk is larger than the compartment. The fixed normalized total solute amount $\Phi_{\text{tot}} = N_{\text{tot}} \nu_c / V_c$ denotes the fraction of the compartment occupied by solute if the bulk was empty. Note that this fraction can exceed 1 if there is more material than can fit in the compartment.

The equilibrium behavior of the system is governed by the total free energy,

$$F = \int_{V_c} f_c(\phi_1, \phi_2) d^n r + \int_{V_b} f_b(\psi_1, \psi_2) d^m r, \quad (3)$$

where we consider the free energy densities

$$f_c = \frac{k_B T}{\nu_c} \left[\phi_1 \ln(\phi_1) + \frac{\phi_2}{2} \ln(\phi_2) + (1 - \phi) \ln(1 - \phi) + \omega_{1,c} \phi_1 + \omega_{2,c} \phi_2 + \chi \phi(1 - \phi) \right], \quad \text{and} \quad (4a)$$

$$f_b = \frac{k_B T}{\nu_b} \left[\psi_1 \ln(\psi_1) + \frac{\psi_2}{2} \ln(\psi_2) + (1 - \psi) \ln(1 - \psi) + \omega_{1,b} \psi_1 + \omega_{2,b} \psi_2 + \chi \psi(1 - \psi) \right], \quad (4b)$$

which each account for translational entropy (respective first three terms), contributions of monomers (fourth term) and dimers (fifth term), as well as an unspecific interaction between all solute molecules captured by the Flory parameter χ [31, 32]. For simplicity, we assume that the unspecific interactions are the same in both subsystems. Likewise, we assume that dimerization and compartment binding are decoupled, so that the total energy decreases by ω_2 when a solute molecule becomes part of a dimer, independent of the subsystem it is in. This also implies that the energy $\Delta\omega$ gained when a solute molecule enters the compartment is independent of whether this molecule is part of a dimer. This

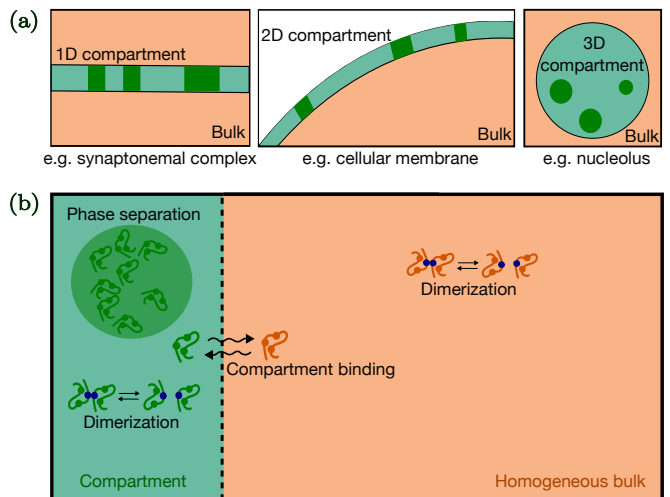


FIG. 1. **Schematic picture of the equilibrium model.**

(a) Examples of phase separation in compartments of different dimensions coupled to a large bulk. (b) Our model describes potential dimerization (ω_2), compartment binding ($\Delta\omega$), and unspecific interactions (χ) leading to phase separation in the compartment, while the large bulk stays homogeneous.

choice implies $\omega_{1,b} = 0$, $\omega_{2,b} = -\omega_2$, $\omega_{1,c} = -\Delta\omega$, and $\omega_{2,c} = -\omega_2 - \Delta\omega$. Taken together, there are five independent parameters: η determines the relative sizes of the compartment, Φ_{tot} sets the total amount of material, and the three interaction energies ω_2 , $\Delta\omega$, and χ govern the tendency of the solute to dimerize, be located in the compartment, and phase separate, respectively; see Fig. 1b.

III. RESULTS

A. Dimerization regulates compartment binding

We first study the interplay between dimerization and compartment binding, neglecting unspecific interactions ($\chi = 0$). In this case, phase separation cannot take place and both subsystems remain homogeneous, so the free energy F given by Eq. (3) only depends on the average fractions ϕ_1 , ϕ_2 , ψ_1 , and ψ_2 . At equilibrium, F is minimized under the material-conservation constraint given by Eq. (2). We minimize F by first minimizing the two terms in Eq. (3) separately, which corresponds to equilibrating the dimerization reaction. We can then express the monomer fraction $\bar{\phi}_1$ and the dimer fraction $\bar{\phi}_2$ in the compartment as a function of the total fraction $\bar{\phi}$,

$$\bar{\phi}_1 = \frac{(1 + 4K_d \bar{\phi})^{\frac{1}{2}} - 1}{2K_d}, \quad \bar{\phi}_2 = \bar{\phi} - \bar{\phi}_1, \quad (5)$$

introducing the dimerization constant $K_d = e^{2\omega_2+1}$ governing the dimerization equilibrium, $\bar{\phi}_2/\bar{\phi}_1^2 = K_d$; see App. A. Eq. (5) implies that the compartment is dominated by monomers in the limit $K_d \bar{\phi} \ll 1$, whereas it

contains mostly dimers when $K_d \bar{\phi} \gg 1$. Moreover, $\bar{\phi}_2$ increases faster than $\bar{\phi}_1$ as a function of the total fraction $\bar{\phi}$, implying that the ratio of dimers increases with $\bar{\phi}$; see Fig. 2a. Analogous expressions apply for the fractions $\bar{\psi}_1$, $\bar{\psi}_2$, and $\bar{\psi}$ in the bulk. For both subsystems, we can then express the free energy density as a function of $\bar{\phi}$ and $\bar{\psi}$ alone. Since these two quantities are linked by the constraint given by Eq. (2), we can express F as a function of only the bulk fraction $\bar{\psi}$. Minimizing F with respect to $\bar{\psi}$ then yields the global equilibrium, where the dimerization in each subsystem and compartment binding are equilibrated.

We start by discussing the limiting cases of mostly monomers ($\omega_2 \rightarrow -\infty$). In this case, we have $\bar{\phi}_1 = \bar{\phi}$ and $\bar{\psi}_1 = \bar{\psi}$, whereas $\bar{\phi}_2 = \bar{\psi}_2 = 0$. If the bulk is dilute ($\bar{\psi}_1 \ll 1$), we find $\bar{\phi}_1/\bar{\psi}_1 \approx (1 - \bar{\phi}_1)e^{\Delta\omega}$. If the compartment is also dilute ($\bar{\phi}_1 \ll 1$), this implies that the ratio $\bar{\phi}_1/\bar{\psi}_1$ is given by $e^{\Delta\omega}$; see Fig. 2b. However, if the overall amount of material increases sufficiently ($\Phi_{\text{tot}} > \frac{1}{2} + \eta e^{-\Delta\omega}$), the compartment is more than half filled ($\bar{\phi}_1 > \frac{1}{2}$), and the ratio $\bar{\phi}_1/\bar{\psi}_1$ significantly decreases below $e^{\Delta\omega}$. For much larger Φ_{tot} , the compartment saturates, so that excess amount is constrained to the bulk. In the opposing limit of mostly dimers ($\omega_2 \rightarrow \infty$), we find $\bar{\phi}_1 = \bar{\psi}_1 = 0$, and $\bar{\phi}_2/\bar{\psi}_2 = (1 - \bar{\phi}_2)^2 e^{2\Delta\omega}$, implying an increased affinity toward the compartment compared to the monomeric case ($\bar{\phi}_2/\bar{\psi}_2 > \bar{\phi}_1/\bar{\psi}_1$); see Fig. 2b. Note that this increased affinity can be interpreted in two complementary pictures: Focusing on individual particles, dimerization reduces their translational entropy, and thus the overall free energy, implying that dimers are favored. In contrast, if we focus on the number concentrations of monomers and dimers, we simply find that the binding energy of dimers is twice that of monomers, explaining their increased affinity. Taken together, binding and dimerization increase the fractions ϕ_i in the compartment until saturation is reached.

We next focus on the intermediate case, where monomers and dimers can both be present in significant amounts. For instance, in the case of $\omega_2 = 3$, Fig. 2b shows that the total fractions $\bar{\phi}$ and $\bar{\psi}$ in the two subsystems transition from the monomeric limit to the dimeric limit when the total fraction Φ_{tot} is increased. This transition is a consequence of the preferred binding toward the compartment and the non-linear response of dimerization: If the total fraction Φ_{tot} is low, both subsystems contain mostly monomers; see Eq. (5) and Fig. 2a. Since the fraction in the compartment is larger than the fraction in the bulk ($\bar{\phi} > \bar{\psi}$), the compartment contains more dimers than the bulk, and will thus eventually transition into a state dominated by dimers while the bulk is still dominated by monomers. Finally, for sufficiently large Φ_{tot} , the bulk will also contain mostly dimers and the transition is completed. These three phases are summarized in Fig. 2c, indicating that we can predict the transition points by appropriate equilibration of the limiting cases; see App. B. Note that the saturation of the compartment implies another non-linearity for very large

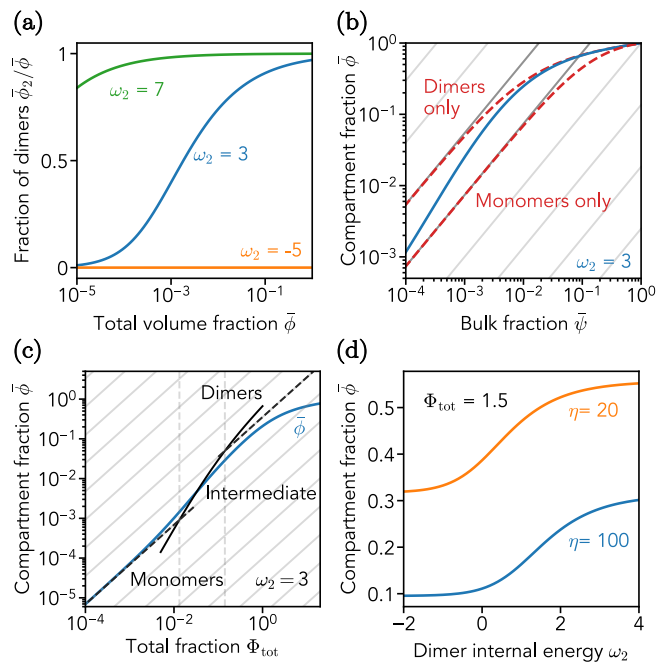


FIG. 2. Dimerization regulates compartment binding. (a) Fraction $\bar{\phi}_2$ of dimers normalized to total fraction $\bar{\phi}$ as a function of $\bar{\phi}$ for a single compartment for various dimerization energies ω_2 . (b) $\bar{\phi}$ in the compartment as a function of the total fraction $\bar{\psi}$ in the bulk for $\omega_2 = 3$. The predictions for systems exclusively comprising monomers and dimers are shown as red dashed lines. (c) $\bar{\phi}$ as a function of the total fraction Φ_{tot} in the system for $\omega_2 = 3$. The three scaling regimes discussed in the main text are highlighted by black lines. (d) $\bar{\phi}$ as a function of ω_2 for various η at $\Phi_{\text{tot}} = 1.5$. (a)–(d) Additional model parameters are $\eta = 100$ and $\Delta\omega = 2$.

Φ_{tot} . Taken together, the interplay between dimerization and compartment binding leads to non-linear behavior, suggesting that dimerization, as well as the relative size η , can be used to control compartment binding (see Fig. 2d).

B. Dimerization facilitates phase separation

We next investigate how dimerization affects phase separation in the simple situation where the bulk is negligible ($\Delta\omega \rightarrow \infty$). Since we now allow for phase separation ($\chi \neq 0$), the compartment can be heterogeneous and its state is described by the fields $\phi_1(\mathbf{r})$ and $\phi_2(\mathbf{r})$. However, the dimerization equilibrium, $\delta F/\delta\phi_1 = \delta F/\delta\phi_2$, holds everywhere, allowing us to express these fields in terms of total fraction $\phi(\mathbf{r})$, analogously to Eq. (5); see App. A. Consequently, the total free energy is given by an integral over a free energy density that only depends on $\phi(\mathbf{r})$, which is analogous to standard binary phase separation [33, 34]. In particular, the compartment can separate into a dense and a dilute phase with identical dimerization equilibrium, $\phi_2/\phi_1^2 = K_d$, if the interaction parameter χ is sufficiently large. Fig. 3a shows that

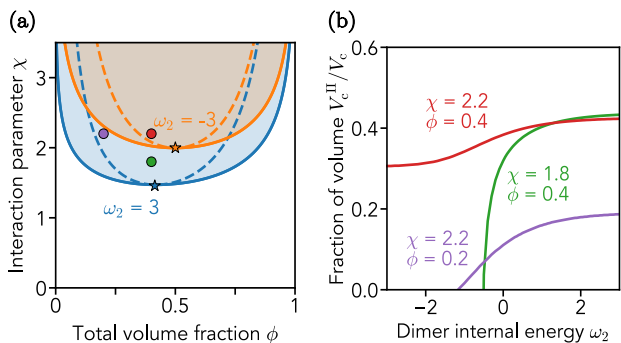


FIG. 3. **Dimerization facilitates phase separation.** (a) Phase diagrams as a function of volume fraction ϕ and interaction strength χ for the two indicated dimerization energies ω_2 . Phase-separated states are stable above the solid binodal lines, whereas the homogeneous state is stable below the dashed spinodal lines. The critical points are marked by stars. (b) Fraction of the volume V_c^{II}/V_c of the dense phase to the compartment volume V_c as a function of ω_2 for three different parameters indicated in the plot and marked in panel (a).

larger χ is required to induce phase separation for smaller ω_2 (smaller K_d). This effect can be understood by analyzing the homogeneous state $\phi(\mathbf{r}) = \bar{\phi}$, which becomes unstable in the spinodal region, $\chi > \chi_{\text{sp}}$, with

$$\chi_{\text{sp}} = \frac{1}{4\bar{\phi}} \left(\frac{1}{(1 + 4K_d\bar{\phi})^{\frac{1}{2}}} + \frac{1 + \bar{\phi}}{1 - \bar{\phi}} \right); \quad (6)$$

see App. A. This expression shows that χ_{sp} increases for smaller $K_d = e^{2\omega_2+1}$. This effect is stronger for smaller $\bar{\phi}$, implying that smaller ω_2 move the spinodal region toward large total fractions; see Fig. 3a. This behavior can also be understood from the limiting case of only monomers ($\omega_2 \rightarrow -\infty$) and only dimers ($\omega_2 \rightarrow \infty$): In terms of the Flory-Huggins theory [32] the only difference between these two cases is the contribution to translational entropy, which is halved for the dimers. Consequently, a smaller enthalpic gain by the unspecific interaction χ can offset the entropic loss of concentrating particles in a phase. The minimal value of χ necessary to obtain phase separation can be calculated by minimizing $\chi_{\text{sp}}(\bar{\phi})$ given by Eq. (6), which corresponds to the critical point (stars in Fig. 3a). For monomers ($\omega_2 \rightarrow -\infty$), we obtain $\chi_{\text{sp}}^{\text{min}} = 2$, whereas $\chi_{\text{sp}}^{\text{min}} = (3 + 2\sqrt{2})/4 \simeq 1.46$ for dimers ($\omega_2 \rightarrow \infty$). Taken together, this analysis shows that the dimerization energy ω_2 can control phase separation and droplet size; see Fig. 3b.

C. Sequestration by the bulk suppresses phase separation in the compartment

We next study phase separation in the compartment coupled to the bulk without dimerization (only monomers, $\omega_2 \rightarrow -\infty$). We focus on the case where particles prefer the compartment ($\Delta\omega > 0$) since in the

opposing case the smaller compartment would be negligible compared to the bulk. In this case, the average fraction $\bar{\phi}$ in the compartment is larger than the fraction $\bar{\psi}$ in the bulk, favoring phase separation in the compartment. The bulk would only phase separate if the total fraction Φ_{tot} is very large, at which point the compartment is saturated. In this case, the compartment would only sequester a fixed amount of material, but not influence phase separation further. More generally, at most one of two coupled subsystems can exhibit phase separation in equilibrium [13–15, 30], and we thus focus on the case where the compartment is favored ($\Delta\omega > 0$) and the bulk remains homogeneous with a fraction $\bar{\psi}$. In this case, the bulk can be approximated as a dilute mixture, so the chemical potentials in the compartment, $\mu_c = \delta F/\delta\phi$, and the bulk, $\mu_b = \partial F/\partial\bar{\psi}$, read

$$\mu_c(\phi) = \ln\left(\frac{\phi}{1-\phi}\right) - \Delta\omega + \chi(1-2\phi), \quad (7a)$$

$$\mu_b(\bar{\psi}) \approx \ln(\bar{\psi}) + \chi, \quad (7b)$$

for $\bar{\psi} \ll 1$. Using material conservation given by Eq. (2) to eliminate $\bar{\psi}$ in Eq. (7b), and shifting both chemical potentials by $\ln\eta - \chi$, we find

$$\mu_c^{\text{eff}}(\phi) = \ln\left(\frac{\phi}{1-\phi}\right) - \Delta\omega_{\text{eff}} - 2\phi\chi, \quad (8a)$$

$$\mu_b^{\text{eff}}(\bar{\phi}) \approx \ln(\Phi_{\text{tot}} - \bar{\phi}), \quad (8b)$$

where $\Delta\omega_{\text{eff}} = \Delta\omega - \ln\eta$ captures the enthalpy and entropy gained when a solute particle moves from the bulk to the compartment. It shows that the relative size η of the subsystems plays a similar role to the compartment affinity $\Delta\omega$. In particular, in the limit of a small bulk ($\eta \rightarrow 0$), we find $\Delta\omega_{\text{eff}} \rightarrow \infty$, so that all solute particles go to the compartment ($\bar{\phi} \rightarrow \Phi_{\text{tot}}$). In this case, the bulk becomes negligible, and the behavior in the compartment is governed by ordinary phase separation in the canonical ensemble. In the contrasting case of a large bulk ($\eta \rightarrow \infty$), implying $\Delta\omega_{\text{eff}} \rightarrow -\infty$, we also need to increase the total fraction Φ_{tot} to have solutes in the compartment. This implies $\Phi_{\text{tot}} \gg \bar{\phi}$, so that $\bar{\phi}$ is negligible in Eq. (8b), implying constant μ_b , which corresponds to a grand-canonical ensemble for the compartment. The interesting case of a bulk of finite size thus interpolates between these two traditional ensembles.

Fig. 4a shows how the phase diagram depends on the effective affinity $\Delta\omega_{\text{eff}}$. In the limit of large $\Delta\omega_{\text{eff}}$ (blue lines), we indeed recover the canonical phase diagram of a binary system since the bulk is almost empty $\bar{\psi} \approx 0$, whereas the total fraction $\bar{\phi}$ in the compartment approaches the total fraction Φ_{tot} . Phase separation can thus take place in the binodal region, where Φ_{tot} is between the fractions ϕ^{I} and ϕ^{II} of the dilute and dense phase in the compartment, $\Phi_{\text{tot}} \in (\phi^{\text{I}}, \phi^{\text{II}})$. For smaller $\Delta\omega_{\text{eff}}$ the entire phase diagram shifts toward larger Φ_{tot} (orange lines), essentially because a significant fraction of solute molecules is in the bulk. In particular,

phase separation only occurs in the compartment when $\Phi_{\text{tot}} \in (\Phi_{\text{tot}}^{\min}, \Phi_{\text{tot}}^{\max})$; see Fig. 4a for an example at $\chi = 3$. However, the coexisting fractions in the dilute and dense phase in the compartment are still given by ϕ^I and ϕ^{II} (see App. C), and thus need to be read off the phase diagram corresponding to the canonical ensemble (blue lines). In essence, the phase diagram as a function of Φ_{tot} determines what total fractions lead to phase separation, whereas the coexisting volume fractions $\phi^{I/II}$ need to be determined from the canonical phase diagram as a function of $\bar{\phi}$. We show in App. C that the difference between these fractions are

$$\Phi_{\text{tot}}^{\min} - \phi^I = \Phi_{\text{tot}}^{\max} - \phi^{II} = e^{-\Delta\omega_{\text{eff}} - \chi}, \quad (9)$$

because the bulk sequesters a constant fraction of material when the compartment phase separates; see Fig. 4b. In essence, phase coexistence in the compartment determines the fractions $\phi^{I/II}$, with equal chemical potentials between the two phases and the bulk. Changing Φ_{tot} then only changes the relative sizes of the two phases according to the lever rule, leaving all fractions unchanged. Eq. (9) shows that the fraction of material sequestered by the bulk decreases with larger effective affinity $\Delta\omega_{\text{eff}}$ and larger interaction strength χ , so that the phase diagram approaches the canonical limit for large $\Delta\omega_{\text{eff}} + \chi$.

Bulk sequestration changes the phase diagram qualitatively. For instance, we find a re-entrant phase transition when changing the interaction parameter χ . Fig. 4a shows an example for $\Delta\omega_{\text{eff}} = -2$ (orange lines) where phase separation is only possible in a narrow regime of χ when Φ_{tot} is equal to the marked Φ_{tot}^{\max} . This is essentially due to an increasing fraction $\bar{\phi}$ in the compartment when χ increases, caused by the lower chemical potential; see Eq. (8a). Similarly, $\bar{\phi}$ increases monotonically (and $\bar{\psi}$ decreases accordingly) for larger affinity $\Delta\omega$ or smaller size ratio η . In contrast, the total fraction Φ_{tot} affects the system differently; see Fig. 4b. While $\bar{\phi}$ and $\bar{\psi}$ increase with Φ_{tot} if the compartment is homogeneous (outside the binodal), only the size of the dense phase increases, but the fractions stay constant, when the compartment phase separates, which is akin to noise buffering described in simple phase separation [35]. Taken together, we show that the affinity $\Delta\omega$, the size ratio η , and the interaction strength χ can be used to control phase separation in the compartment together with the total amount Φ_{tot} .

We next discuss the stability of homogeneous states to distinguish nucleation and growth regimes from spinodal decomposition. Fig. 4c shows that the spinodal (dashed orange line) also moves toward larger total fractions Φ_{tot} for smaller $\Delta\omega_{\text{eff}}$, similarly to the binodals discussed above. In this case, the entire phase diagram is thus qualitatively similar to the phase diagram in the canonical limit ($\Delta\omega_{\text{eff}} \rightarrow \infty$). In contrast, phase diagrams for smaller $\Delta\omega_{\text{eff}}$, where the compartment is less favored, can be qualitatively different; see Fig. 4d. In this case, the spinodal decomposition region is reduced dramatically, and the two nucleation-and-growth regimes

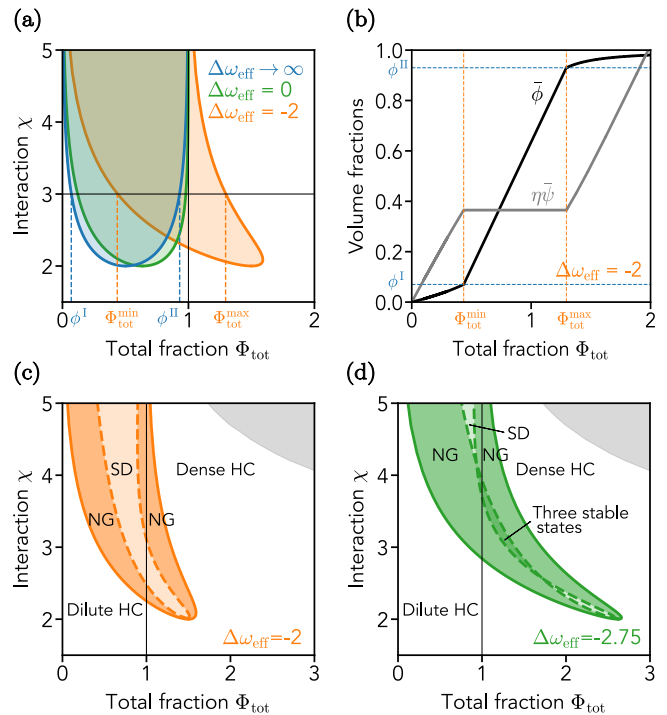


FIG. 4. Sequestration by the bulk suppresses phase separation in the compartment. (a) Phase diagrams as a function of the total fraction Φ_{tot} and interaction strength χ for two effective affinities $\Delta\omega_{\text{eff}} = \Delta\omega - \ln \eta$. The compartment can phase separate within the colored regions. The limit of strong binding (blue) recovers the canonical phase diagram, determining the coexisting volume fractions ϕ^I and ϕ^{II} (plot shows example for $\chi = 3$). Weaker binding (green and orange) moves the region to larger Φ_{tot} and the intersections with the line $\chi = 3$ now give the region $\Phi_{\text{tot}} \in (\Phi_{\text{tot}}^{\min}, \Phi_{\text{tot}}^{\max})$ where phase separation takes place, whereas the coexisting volume fractions still correspond to $\phi^{I/II}$. (b) Average volume fractions $\bar{\phi}$ in the compartment and normalized fraction $\eta\bar{\psi}$ in the bulk as a function of Φ_{tot} for $\Delta\omega_{\text{eff}} = -2$. (c, d) Phase diagrams including spinodals (dashed lines) for two values of $\Delta\omega_{\text{eff}}$, separating spinodal decomposition (SD) from the nucleation-and-growth (NG) region. White regions denote a globally stable homogeneous configuration (HC), whereas HCs are only linearly stable in the darker region between the dashed and solid lines, leading to multistability in the central region of panel (d). The bulk exhibits phase separation in the gray region for $\eta = 100$.

overlap. In this overlap region (dark green), there are three stable states: the phase separated state has the lowest free energy, but there are also two locally stable homogeneous states. This is because the binding equilibrium, $\mu_c(\bar{\phi}) = \mu_b(\bar{\phi})$ using Eqs. (8), leads to a non-linear equation with three solutions, of which two are stable; see App. C. We thus showed that a medium-sized bulk can affect phase separation qualitatively, leading to the effective binding affinity $\Delta\omega_{\text{eff}} = \Delta\omega - \ln \eta$ as a central control parameter.

D. Dimerization and bulk sequestration jointly regulate compartment phase separation

We finally combine all effects to understand how phase separation in the compartment could be regulated. Fig. 5a–b show examples for phase diagrams for various dimerization energies ω_2 and binding affinities $\Delta\omega$. In essence, we find a combination of the effects obtained from the individual considerations above: Favoring dimers (larger ω_2) reduces the interaction χ required for phase separation, similar to the results shown in Fig. 3. In contrast, bulk sequestration moves the binodal region to larger total fractions Φ_{tot} , analogous to Fig. 4. This again implies a parameter regime where three states are stable (dark orange region in Fig. 5b) for low $\Delta\omega$. The same regime also emerges when the dimerization energy ω_2 is reduced (see Fig. 2d) or η is increased. This suggests that the three parameters $\Delta\omega$, ω_2 , and η effectively control the tendency of the material to be in the compartment.

We find that all parameters in the system can be used to control whether the compartment phase separates and what fraction V_c^{II}/V_c is occupied by the dense phase; see Fig. 5c. The fraction of volume V_c^{II}/V_c generally increases with increasing $\Delta\omega$, ω_2 , Φ_{tot} , and χ . The plots also reveal various phase transitions, including re-entrant transitions where increasing a parameter (for instance $\Delta\omega$ in the upper right panel) induces a transition from a dilute homogeneous phase to a phase separated state, and then a dense homogeneous state.

IV. DISCUSSION

Our equilibrium theory provides a comprehensive summary of the interplay of dimerization, compartment binding, and phase separation. In the simplest cases, we can understand phase separation in the compartment by treating the bulk as a perturbation: The bulk sequesters a certain fraction of material, lowering the available fraction in the compartment, which is relevant for phase separation. The sequestration depends on the size ratio η , the binding affinity $\Delta\omega$, the dimerization energy ω_2 , and the interaction parameter χ . However, since ω_2 and χ also directly affect phase separation, there can be an intricate interplay between sequestration and phase separation, which for instance leads to the three stable states shown in Fig. 4d and Fig. 5b. This multistability could in principle be observed in small compartments (e.g., lipid droplets [8], the synaptomenal complex during meiosis [5], or yeast vacuoles [36]).

We showed that dimerization plays a double role since it lowers the interaction energy χ required for phase separation (see Fig. 3a) and it increases the effective affinity toward the compartment (see Fig. 2). Both these roles can either be interpreted as halving the entropy of molecules that are bound in dimers or as doubling enthalpic contributions when comparing monomers to

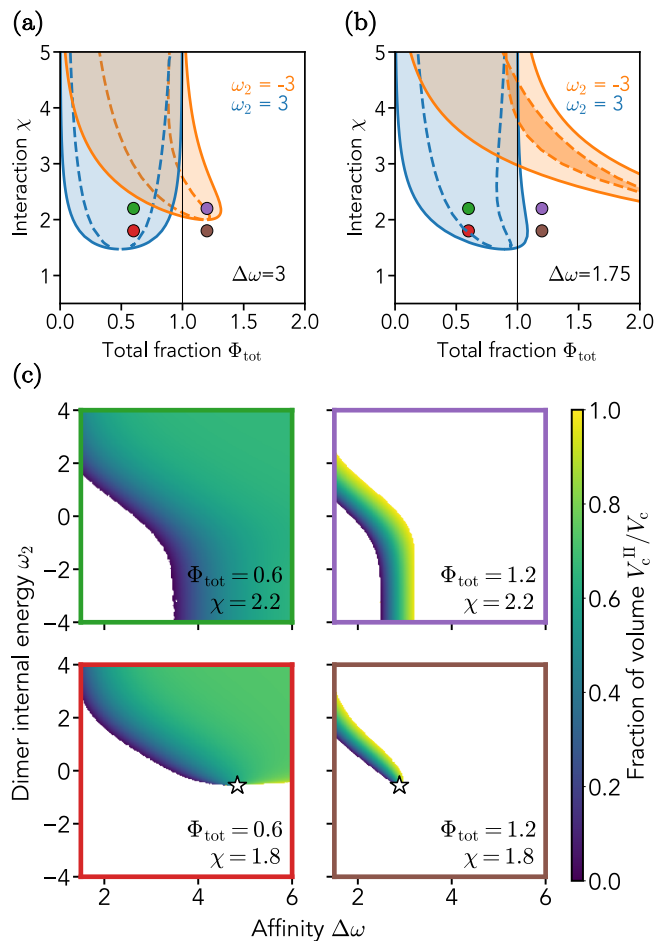


FIG. 5. Dimerization and bulk sequestration jointly regulate compartment phase separation (a)–(b) Phase diagrams as a function of the total fraction Φ_{tot} and interaction strength χ for two dimerization energies ω_2 and different compartment affinities $\Delta\omega$. The compartment can phase separate within the colored regions. Dashed spinodal lines mark the stability of homogeneous states; the dark orange region in (b) indicates that both homogeneous states are stable. (c) Volume V_c^{II} of the dense phase normalized to compartment volume V_c as a function of $\Delta\omega$ and ω_2 for various Φ_{tot} and χ as indicated. Critical points are marked by stars. (a)–(c) Phase diagrams have been determined numerically; The size ratio is $\eta = 100$.

dimers. These effects amplify existing energy differences between subsystems, so that even small affinities can concentrate most of the material in a compartment (see Fig. 2d). If multiple subsystems compete with each other, this mechanism allows to target the most favored subsystem reliably. For these reasons, and because dimerization is ubiquitous, it is plausible that cells exploit dimerization as a regulation mechanism [18]. Moreover, the same principles apply for higher-order oligomers, which are also known to affect protein localization in cells [19, 20, 37]

The multistability of homogeneous states and the amplification by oligomerization vanishes when one subsys-

tem is much larger than the other. When the bulk is small, the compartment can be described using a canonical ensemble; the opposing limit corresponds to a grand-canonical ensemble, where the large bulk plays the role of a chemostat. Our model reveals complex behavior between these classical limiting cases. Similar quantitative dependencies on the size ratio of subsystems were found experimentally studying the PAR protein system [38, 39] and the Min protein oscillations [40, 41], suggesting that it might be another important control parameter in cells.

Our equilibrium theory captures basic ingredients that allow regulating phase separation in a compartment. The theory can be naturally extended to include multiple components, mechanical degrees of freedom (like membrane fluctuations [42], membrane curvature [43, 44], receptor binding [45], or bulk elasticity [46]), and activity (using open systems [47, 48], or driven reactions [27, 34, 49]). Those ingredients can help to regulate phase separation in the compartment, which could for instance explain polarity patterns in membranes [23–25].

ACKNOWLEDGMENTS

We thank Liedewij Laan, Nynke Hetteema, Marieke Glazenburg, Zhiheng Wu, Nathan Goehring, Tom Bland, Marcel Ernst, and Kueyoung Kim for helpful discussions. We gratefully acknowledge funding from the Max Planck Society and the European Union (ERC, Emul-Sim, 101044662). GW acknowledges funding through a fellowship of the IMPRS for Physics of Biological and Complex Systems.

Appendix A: Dimerization equilibrium

The free energy density of a single subsystem with a monomer fraction ϕ_1 and dimer fraction ϕ_2 reads

$$\frac{f(\phi_1, \phi_2)\nu}{k_B T} = \phi_1 \ln(\phi_1) + \frac{\phi_2}{2} \ln(\phi_2) + (1 - \phi) \ln(1 - \phi) + \omega_1 \phi_1 + \omega_2 \phi_2. \quad (\text{A1})$$

Combining particle conservation, $\phi_1 + \phi_2 = \phi$, with the dimerization equilibrium, $\partial f / \partial \phi_1 = \partial f / \partial \phi_2$, [50]

$$\phi_1 = \frac{-1 + \sqrt{1 + 4K_d \phi}}{2K_d} \quad \phi_2 = \phi - \phi_1 \quad (\text{A2})$$

with the dimerization constant $K_d = \phi_2 / \phi_1^2$ given by $K_d = e^{2(\omega_2 + 1)}$. Inserting these relations in Eq. (A1) results in an effective free energy that only depends on ϕ , implying the effective chemical potential $\mu = \nu \partial f / \partial \phi$. The spinodal condition, $f''(\phi) = 0$, then implies

$$\chi_{\text{sp}} = \frac{1}{4\bar{\phi}} \left(\frac{1}{\sqrt{1 + 4K_d \bar{\phi}}} + \frac{1 + \bar{\phi}}{1 - \bar{\phi}} \right). \quad (\text{A3})$$

Appendix B: Limiting cases of dimerization equilibrium in coupled subsystems

We first consider the limiting case of only monomers, focusing on dilute systems for simplicity. In equilibrium, the compartment fraction $\bar{\phi}$ then reads

$$\bar{\phi}_{\text{mono}} = \frac{\bar{\Phi}_{\text{tot}} e^{\Delta\omega}}{\eta + e^{\Delta\omega}}. \quad (\text{B1})$$

In the case of dilute systems filled with dimers, we find

$$\bar{\phi}_{\text{dim}} = \frac{\bar{\Phi}_{\text{tot}} e^{2\Delta\omega}}{\eta + e^{2\Delta\omega}}. \quad (\text{B2})$$

In the intermediate regime, we consider the compartment to only contain dimers, whereas the bulk only has monomers, leading to

$$\bar{\phi}_{\text{int}} = \frac{e^{-(1+2(\omega_2+\Delta\omega))}}{2} \left[\eta^2 + 2e^{1+2(\omega_2+\Delta\omega)} \bar{\Phi}_{\text{tot}} - \eta \sqrt{\eta^2 + 4e^{1+2(\omega_2+\Delta\omega)} \bar{\Phi}_{\text{tot}}} \right]. \quad (\text{B3})$$

The transitions between these limiting cases take place when $\bar{\phi}_{\text{mono}} = \bar{\phi}_{\text{int}}$ and $\bar{\phi}_{\text{int}} = \bar{\phi}_{\text{dim}}$, leading to the two respective transition points

$$\bar{\Phi}_{\text{tot,mono}} = \frac{e^{\Delta\omega} + \eta}{e^{1+2\omega_2+\Delta\omega}} \quad \bar{\Phi}_{\text{tot,dim}} = \frac{e^{2\Delta\omega} + \eta}{e^{1+2\omega_2}}. \quad (\text{B4})$$

Appendix C: Phase separation in a compartment exchanging material with the bulk

The free energy of a phase separated compartment in contact with a homogeneous bulk reads

$$F = V_c^{\text{I}} f_c(\phi^{\text{I}}) + V_c^{\text{II}} f_c(\phi^{\text{II}}) + V_b f_b(\psi), \quad (\text{C1})$$

subject to the conservation laws $V_c^{\text{I}} + V_c^{\text{II}} = V_c$, $V_c^{\text{I}} \phi^{\text{I}} + V_c^{\text{II}} \phi^{\text{II}} = V_c \phi$, and $\eta \psi + \phi = \bar{\Phi}_{\text{tot}}$, where $\eta = V_b \nu_c / V_c \nu_b$. The necessary conditions for the minimum of F thus read

$$\frac{V_b}{V_c \eta} f'_b(\psi) = f'_c(\phi^{\text{I}}) = f'_c(\phi^{\text{II}}) = \frac{f_c(\phi^{\text{I}}) - f_c(\phi^{\text{II}})}{\phi^{\text{I}} - \phi^{\text{II}}}. \quad (\text{C2})$$

We can simplify these conditions to

$$\tilde{f}'_b(\psi) = \tilde{f}'_c(\phi^{\text{I}}) = \tilde{f}'_c(\phi^{\text{II}}) = 0 \quad (\text{C3})$$

by defining effective free energy densities,

$$\tilde{f}_c = \frac{k_B T}{\nu_c} \left(\phi \ln(\phi) + (1 - \phi) \ln(1 - \phi) + \chi \phi (1 - \phi) \right) \quad (\text{C4a})$$

$$\tilde{f}_b = \frac{k_B T}{\nu_b} \left(\psi \ln(\psi) + (\Delta\omega + \chi - 1) \psi \right), \quad (\text{C4b})$$

with $\Delta\omega = \omega_b - \omega_c$. The first identity in Eq. (C3) implies

$$\frac{V_c^I}{V_c} = \frac{1}{\phi^I - \phi^{II}} \left(\Phi_{\text{tot}} - \phi^{II} - \eta e^{-\Delta\omega - \chi} \right), \quad (\text{C5})$$

and we can determine ϕ^I and ϕ^{II} from the two solutions of the second identity in Eq. (C3),

$$\chi_{\text{bin}} = \frac{1}{2\phi - 1} \ln \left(\frac{\phi}{1 - \phi} \right). \quad (\text{C6})$$

Consequently, the coexisting fractions only depend on χ , implying they can be read off the canonical phase diagram. The region of Φ_{tot} where phase separation happens is then given by $V_c^I \in (0, V_c)$, so that Eq. (C5) implies

$$\Phi_{\text{tot}}^{\text{min}} = \phi^I + \eta e^{-\Delta\omega - \chi} \quad (\text{C7a})$$

$$\Phi_{\text{tot}}^{\text{max}} = \phi^{II} + \eta e^{-\Delta\omega - \chi}. \quad (\text{C7b})$$

Since the chemical potentials are all constant, the bulk fraction $\psi = \exp(-\Delta\omega - \chi)$ is a constant in the region where the compartment phase separates.

The compartment is homogeneous in equilibrium when $\mu_c(\phi^*) = \mu_b(\psi^*)$. To see whether this state is stable, we test whether the perturbed state $\phi(\mathbf{r}) = \phi^* + \delta\phi(\mathbf{r})$

increases the total free energy

$$F[\phi, \psi] = V_b f_b(\psi) + \int_{V_c} f_c(\phi) dV_c, \quad (\text{C8})$$

assuming a homogeneous bulk. The first variation of the free energy, $\delta F[\phi] = F[\phi] - F[\phi^*]$, reads

$$\delta F[\phi] = \int_{V_c} \left[f'_c(\phi^*) \delta\phi + \frac{f''_c(\phi^*)}{2} \delta\phi^2 \right] dV_c + V_b \left(f'_b(\psi^*) \delta\psi + \frac{f''_b(\psi^*)}{2} \delta\psi^2 \right). \quad (\text{C9})$$

Material conservation, given by Eq. (1), implies

$$\delta\psi(t) = -\frac{1}{\eta} \int_{V_c} \frac{\delta\phi(\mathbf{r}, t)}{V_c} dV_c. \quad (\text{C10})$$

The terms proportional to $\delta\phi$ and $\delta\psi$ thus cancel in Eq. (C9). We express remaining terms in Fourier space,

$$\delta F[\hat{\phi}] = V_c \int d^n q \left[\frac{f''_c(\phi^*)}{2} \hat{\phi}(\mathbf{q})^2 \right] + \frac{V_b}{2\eta^2} f''_b(\psi^*) \hat{\phi}(\mathbf{0})^2. \quad (\text{C11})$$

If the bulk is stable, $f''_b(\psi^*) > 0$, the second term increases δF , implying that the homogeneous state is stable if the first term is positive, i.e., if $f''_c(\phi^*) > 0$.

To estimate when the bulk would become unstable, we check whether its fraction ψ lies within the binodal region. The gray region in Fig. 4 marks such regions.

-
- [1] A. A. Hyman, C. A. Weber, and F. Jülicher, Liquid-liquid phase separation in biology, *Annual Review of Cell and Developmental Biology* **30**, 39 (2014).
- [2] O. Rog, S. Köhler, and A. F. Dernburg, The synaptonemal complex has liquid crystalline properties and spatially regulates meiotic recombination factors, *eLife* **6**, e21455 (2017).
- [3] C. Morgan, M. A. White, F. C. H. Franklin, D. Zickler, N. Kleckner, and K. Bomblies, Evolution of crossover interference enables stable autopolyploidy by ensuring pairwise partner connections in *Arabidopsis arenosa*, *Current Biology* **31**, 4713 (2021).
- [4] L. Zhang, W. Stauffer, D. Zwicker, and A. F. Dernburg, Crossover patterning through kinase-regulated condensation and coarsening of recombination nodules, *bioRxiv* 10.1101/2021.08.26.457865 (2021).
- [5] S. Durand, Q. Lian, J. Jing, M. Ernst, M. Grelon, D. Zwicker, and R. Mercier, Joint control of meiotic crossover patterning by the synaptonemal complex and *hei10* dosage, *Nature Communications* **13**, 5999 (2022).
- [6] J. A. Morin, S. Wittmann, S. Choubey, A. Klosin, S. Golfier, A. A. Hyman, F. Jülicher, and S. W. Grill, Sequence-dependent surface condensation of a pioneer transcription factor on dna, *Nature Physics* **18**, 271 (2022).
- [7] S. Mukherjee and F. R. Maxfield, Membrane domains, *Annual Review of Cell and Developmental Biology* **20**, 839 (2004).
- [8] A. Kamatar, J. P. Bravo, F. Yuan, L. Wang, E. M. Lafer, D. W. Taylor, J. C. Stachowiak, and S. H. Parekh, Lipid droplets as substrates for protein phase separation, *Biophysical Journal* <https://doi.org/10.1016/j.bpj.2024.03.015> (2024).
- [9] T. Litschel, C. F. Kelley, X. Cheng, L. Babl, N. Mizuno, L. B. Case, and P. Schwill, Membrane-induced 2d phase separation of the focal adhesion protein talin, *Nature Communications* **15**, 4986 (2024).
- [10] Y. Wan, R. Hudson, J. Smith, J. D. Forman-Kay, and J. A. Ditlev, Protein interactions, calcium, phosphorylation, and cholesterol modulate cfr cluster formation on membranes, *bioRxiv* 10.1101/2024.05.03.592454 (2024).
- [11] S. A. Shelby, I. Castello-Serrano, K. C. Wisser, I. Levental, and S. L. Veatch, Membrane phase separation drives responsive assembly of receptor signaling domains, *Nature Chemical Biology* **19**, 750 (2023).
- [12] H. M. Weakly and S. L. Keller, Coupling liquid phases in 3d condensates and 2d membranes: Successes, challenges, and tools, *Biophysical Journal* **123**, 1329 (2024).
- [13] R. Lipowsky, T. Rouhiparkouhi, D. E. Discher, and T. R. Weikl, Domain formation in cholesterol-phospholipid membranes exposed to adhesive surfaces or environments, *Soft Matter* **9**, 8438 (2013).

- [14] P. Fonda, M. Rinaldin, D. J. Kraft, and L. Giomi, Thermodynamic equilibrium of binary mixtures on curved surfaces, *Phys. Rev. E* **100**, 032604 (2019).
- [15] M. Rinaldin, P. Fonda, L. Giomi, and D. J. Kraft, Geometric pinning and antimixing in scaffolded lipid vesicles, *Nature Communications* **11**, 4314 (2020).
- [16] D. L. J. Lafontaine, J. A. Riback, R. Bascetin, and C. P. Brangwynne, The nucleolus as a multiphase liquid condensate, *Nature Reviews Molecular Cell Biology* **22**, 165 (2021).
- [17] W. T. Snead and A. S. Gladfelter, The control centers of biomolecular phase separation: How membrane surfaces, ptms, and active processes regulate condensation, *Molecular Cell* **76**, 295 (2019).
- [18] T. Bland, N. Hirani, D. C. Briggs, R. Rossetto, K. Ng, I. A. Taylor, N. Q. McDonald, D. Zwicker, and N. W. Goehring, Optimized par-2 ring dimerization mediates cooperative and selective membrane binding for robust cell polarity, *The EMBO Journal*, 1 (2024).
- [19] R. Illukkumbura, N. Hirani, J. Borrego-Pinto, T. Bland, K. Ng, L. Hubatsch, J. McQuade, R. G. Endres, and N. W. Goehring, Design principles for selective polarization of PAR proteins by cortical flows, *Journal of Cell Biology* **222**, e202209111 (2023).
- [20] S. Tschirpke, W. K.-G. Daalman, and L. Laan, The *gef cdc24* and *gap rga2* synergistically regulate *cdc42* gtpase cycling, *bioRxiv* 10.1101/2023.06.26.546500 (2023).
- [21] C. F. Lang and E. M. Munro, Oligomerization of peripheral membrane proteins provides tunable control of cell surface polarity, *Biophysical Journal* **121**, 4543 (2022).
- [22] M. S. Turner, P. Sens, and N. D. Socci, Nonequilibrium raftlike membrane domains under continuous recycling, *Phys. Rev. Lett.* **95**, 168301 (2005).
- [23] T. Burkart, M. C. Wigbers, L. Würthner, and E. Frey, Control of protein-based pattern formation via guiding cues, *Nature Reviews Physics* **4**, 511 (2022).
- [24] P. Gross, K. V. Kumar, N. W. Goehring, J. S. Bois, C. Hoegge, F. Jülicher, and S. W. Grill, Guiding self-organized pattern formation in cell polarity establishment, *Nature Physics* **15**, 293 (2019).
- [25] F. Brauns, L. Iñigo de la Cruz, W. K. G. Daalman, I. de Bruin, J. Halatek, L. Laan, and E. Frey, Redundancy and the role of protein copy numbers in the cell polarization machinery of budding yeast, *Nature Communications* **14**, 6504 (2023).
- [26] F. Brauns, J. Halatek, and E. Frey, Diffusive coupling of two well-mixed compartments elucidates elementary principles of protein-based pattern formation, *Phys. Rev. Res.* **3**, 013258 (2021).
- [27] N. Caballero, K. Kruse, and T. Giamarchi, Phase separation on surfaces in the presence of matter exchange, *Phys. Rev. E* **108**, L012801 (2023).
- [28] L. Foret, A simple mechanism of raft formation in two-component fluid membranes, *Europhysics Letters* **71**, 508 (2005).
- [29] X. Zhao, G. Bartolucci, A. Honigmann, F. Jülicher, and C. A. Weber, Thermodynamics of wetting, prewetting and surface phase transitions with surface binding, *New Journal of Physics* **23**, 123003 (2021).
- [30] X. Zhao, S. Liese, A. Honigmann, F. Jülicher, and C. A. Weber, Theory of wetting dynamics with surface binding (2024), [arXiv:2402.10405 \[cond-mat.soft\]](https://arxiv.org/abs/2402.10405).
- [31] P. J. Flory, Thermodynamics of high polymer solutions, *The Journal of Chemical Physics* **10**, 51 (1942).
- [32] M. L. Huggins, Solutions of Long Chain Compounds, *The Journal of Chemical Physics* **9**, 440 (1941).
- [33] C. A. Weber, D. Zwicker, F. Jülicher, and C. F. Lee, Physics of active emulsions, *Reports on Progress in Physics* **82**, 064601 (2019).
- [34] D. Zwicker, The intertwined physics of active chemical reactions and phase separation, *Current Opinion in Colloid & Interface Science* **61**, 101606 (2022).
- [35] A. Klosin, F. Oltsch, T. Harmon, A. Honigmann, F. Jülicher, A. A. Hyman, and C. Zechner, Phase separation provides a mechanism to reduce noise in cells, *Science* **367**, 464 (2020).
- [36] C. L. Leveille, C. E. Cornell, A. J. Merz, and S. L. Keller, Yeast cells actively tune their membranes to phase separate at temperatures that scale with growth temperatures, *Proceedings of the National Academy of Sciences* **119**, e2116007119 (2022).
- [37] U. Rana, K. Xu, A. Narayanan, M. T. Walls, A. Z. Panagiotopoulos, J. Avalos, and C. P. Brangwynne, Asymmetric oligomerization state and sequence patterning can tune multiphase condensate miscibility, *Nature Chemistry* **16**, 1073 (2024).
- [38] L. Hubatsch, F. Peglion, J. D. Reich, N. T. L. Rodrigues, N. Hirani, R. Illukkumbura, and N. W. Goehring, A cell-size threshold limits cell polarity and asymmetric division potential, *Nature Physics* **15**, 1078 (2019).
- [39] R. Gebele, J. Halatek, L. Würthner, and E. Frey, Geometric cues stabilise long-axis polarisation of par protein patterns in *c. elegans*, *Nature Communications* **11**, 539 (2020).
- [40] F. Brauns, G. Pawlik, J. Halatek, J. Kerssemakers, E. Frey, and C. Dekker, Bulk-surface coupling identifies the mechanistic connection between min-protein patterns in vivo and in vitro, *Nature Communications* **12**, 3312 (2021).
- [41] L. Würthner, F. Brauns, G. Pawlik, J. Halatek, J. Kerssemakers, C. Dekker, and E. Frey, Bridging scales in a multiscale pattern-forming system, *Proceedings of the National Academy of Sciences* **119**, e2206888119 (2022).
- [42] Q. Goutaland, F. van Wijland, J.-B. Fournier, and H. Noguchi, Binding of thermalized and active membrane curvature-inducing proteins, *Soft Matter* **17**, 5560 (2021).
- [43] C. Tozzi, N. Walani, and M. Arroyo, Out-of-equilibrium mechanochemistry and self-organization of fluid membranes interacting with curved proteins, *New Journal of Physics* **21**, 093004 (2019).
- [44] F. Yuan, H. Alimohamadi, B. Bakka, A. N. Tremenozzi, K. J. Day, N. L. Fawzi, P. Rangamani, and J. C. Stachowiak, Membrane bending by protein phase separation, *Proceedings of the National Academy of Sciences* **118**, e2017435118 (2021).
- [45] S.-Z. Lin, R. Changede, A. J. Farrugia, A. D. Bershadsky, M. P. Sheetz, J. Prost, and J.-F. m. c. Rupprecht, Membrane tilt drives phase separation of adhesion receptors, *Phys. Rev. Lett.* **132**, 188402 (2024).
- [46] Y. Qiang, C. Luo, and D. Zwicker, Nonlocal elasticity yields equilibrium patterns in phase separating systems, *Phys. Rev. X* **14**, 021009 (2024).
- [47] M. Zamparo, D. Valdembri, G. Serini, I. V. Kolokolov, V. V. Lebedev, L. Dall'Asta, and A. Gamba, Optimality in self-organized molecular sorting, *Phys. Rev. Lett.* **126**, 088101 (2021).
- [48] E. Floris, A. Piras, F. S. Pezzicoli, M. Zamparo, L. Dall'Asta, and A. Gamba, Phase separation and crit-

- ical size in molecular sorting, *Phys. Rev. E* **106**, 044412 (2022).
- [49] J. Kirschbaum and D. Zwicker, Controlling biomolecular condensates via chemical reactions, *Journal of The Royal Society Interface* **18**, 20210255 (2021).
- [50] J. Agudo-Canalejo, P. Illien, and R. Golestanian, Cooperatively enhanced reactivity and “stabilitaxis” of dissociating oligomeric proteins, *Proceedings of the National Academy of Sciences* **117**, 11894 (2020).